Electronic Supplementary Material (ESI) for Nanoscale Horizons.

Supporting Information for

Supramolecular nanocapsules as two-fold stabilizers of outer-cavity sub-nanometric Ru NPs and inner-cavity ultra-small Ru clusters

Ernest Ubasart, Irene Mustieles Marin, Juan Manuel Asensio, Gabriel Mencia, Ángela M. López-Vinasco, Cristina García-Simón, Iker del Rosal, Romuald Poteau,* Bruno Chaudret,* Xavi Ribas*

Table of contents

1. Supplementary Methods

1.1. Materials and Instrumentation

Reagents and solvents were purchased from VWR Prolabo and Sigma-Aldrich. They were dried on alumina desiccant and degassed by passing Ar through for 20 min. Pyrazine was purchased from Sigma Aldrich and used without further purification. Ru(COD)(COT) was purchased from Nanomeps. ESI-MS measurements were performed on a Bruker MicroTOF-Q-II using CH_3CN as a mobile phase. The TEM samples were prepared by dropcast of the solution in a copper grid covered with an amorphous C film, and then dried under vaccum prior to measurement. The TEM images were recorded in a JEOL 1400 microscope working at 120 kV. HR-TEM images were recorded in a probe corrected JEOL ARM Cold-FEG operated at 200 keV.

The catalytic solutions were analyzed by gas chromatography (GC PerkinElmer 580) equipped with a capillary column Elite-5MS (PerkinElmer) and a FID detector and using H_2 as carrier gas. The GC is coupled to a Clarus SQ8T mass spectrometer. Conversion and yields were calculated by comparison of the peak areas of reagent, products and internal standard.

1.2. Procedure for the synthesis of nanocapsules and sub-nanometric nanoparticles

Nanocapsules **6**·$(BArF)_8$ and **8**·$(BArF)_8$ were synthesised following reported methodologies.[1, 2]

The synthesis of Ru NPs was performed in the glove box. For this, 2 mg of nanocapsule were dissolved in 2mL of THF in a Fisher-Porter bottle.[3, 4] To this solution, 324, 199, 149, 100 or 50 µL of a 0.064 M solution of Ru(COD)(COT) (1 mL THF) were added, corresponding to 130, 80, 60, 40 and 20 eq of Ru, respectively. Then 0.2 equivalents of pyrazine with respect to Ru were added, namely 170, 104, 78, 52 or 26 µL of a 0.024 M solution (10mL THF). Finally, 1 mL of THF was added to the solution. The final volume of the solutions was 3.5, 3.3, 3.2, 3.1 and 3.0 mL, respectively. The FP was taken out of the glovebox and charged with 1 bar of H_2. Prior to loading, the line was purged with 3 cycles H_2/vacuum. The solution was stirred for 2 min at room temperature and then the pressure was released. In the case of E12 the same procedure is followed by adding

324 µL of a 0.064 M solution of Ru(COD)(COT) (which corresponds to 130 eq) and 170 µL of a 0.32 M solution of pyrazine (which corresponds to 1 eq). The total volume is 3.5 mL.

For the HRMS-ESI-QTOF analysis, 1 mL of acetonitrile was added to the solution, to solubilize the nanocapsule, followed by two drops of Hg. The mixture was stirred overnight and then filtered to remove the excess of NPs congregated with the Hg (except for E3 and E4).

1.3. Catalytic tests

The catalytic reactions were performed in a Fisher Porter which was load at the air. Different volumes of the Ru NPs solutions were added depending on the Ru equivalents employed in the formation of the NPs; they are specified in Table S1. In all the cases the catalytic loading was 0.25 mol%. To the solutions, 135 µL of styrene (1 mmol) and 227 µL of dodecane (1 mmol), as internal standard, were added. The volume of the solutions was completed to 5.5 mL with THF. In the case of the NPs synthesized employing 20 eq of Ru, 1.5 mL of the Ru NPs solution and 71 µL of styrene were employed, and the total volume of the solution was 3 mL. Then, the line was purged with 3 cycles of H_2/vaccum, the air of the Fisher-Porter was removed, and the Fisher-Porter was loaded with 3 bar of H_2. The mixture was stirred for 5 h at 50 °C. For the GC analysis, 2 drops of the solution were filtered over celite and diluted in 2 mL of THF.

Ru NPs solution	eq. Ru employed	[Ru] mother sol (mM)	V taken (mL)	mol Ru	[Ru] (mM)
E3	130	5.9	0.5	2.9E-06	0.53
E8	130	5.9	0.5	2.9E-06	0.53
E9	80	3.8	0.77	2.9E-06	0.53
E10	60	2.9	1	2.9E-06	0.53
E11	40	2.0	1.46	2.9E-06	0.53
E12	130	5.9	0.5	2.9E-06	0.53
E13*	32	1.0	1.5	1.5E-06	0.53

Table S1. Volumes and concentrations employed in the catalytic mixtures. Total volume of the solutions is 5.5 mL (THF). *Total volume 3 mL.

2. Supplementary Figures

2.1. Ru NPs characterization by TEM and HR-TEM

E1. Pd-pTp (**6**·$(BArF)_8$), 130 eq Ru, 0 eq pyrazine, THF, 10min.

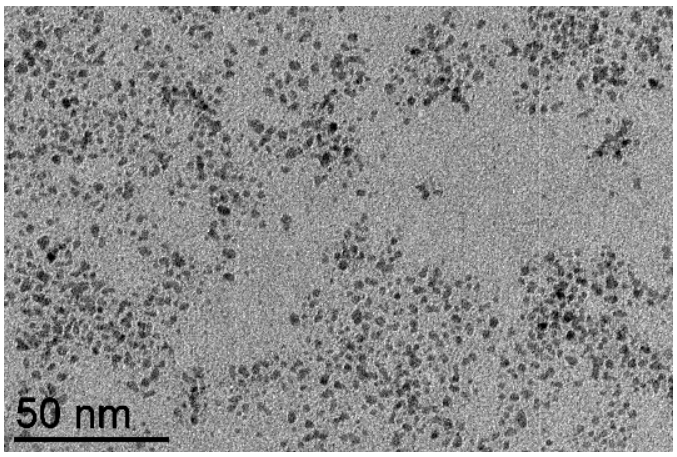

Figure S1. E1. Pd-pTp (**6**·$(BArF)_8$), 130 eq Ru, 0 eq pyrazine, THF, 10min (X120k).

E2. Pd-pTp (**6**·$(BArF)_8$), 130 eq Ru, 0.2 eq pyrazine, THF, 10min.

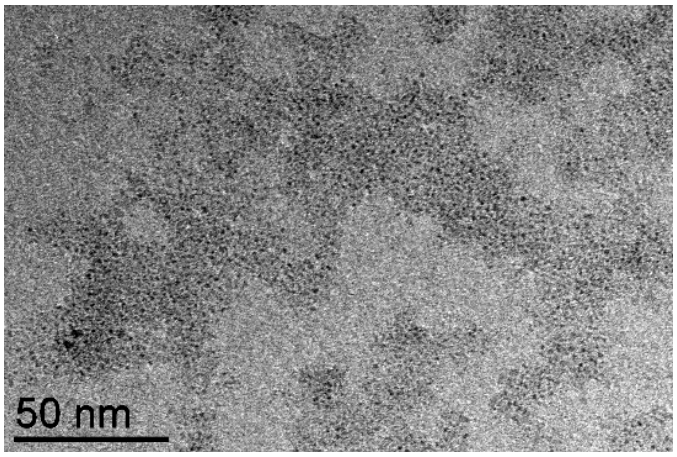

Figure S2. E2. Pd-pTp (**6**·$(BArF)_8$), 130 eq Ru, 0.2 eq pyrazine, THF, 10min (X120k).

E3. Pd-ppp (**8**·$(BArF)_8$), 130 eq Ru, 0 eq pyrazine, THF, 10min.

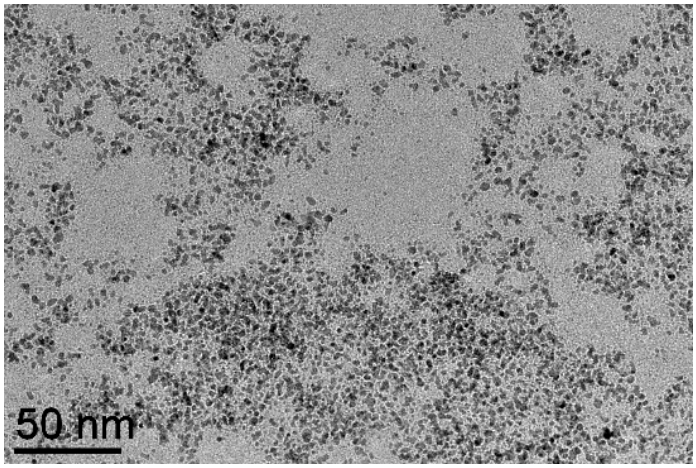

Figure S3. E3. Pd-ppp (**8**·$(BArF)_8$), 130 eq Ru, 0 eq pyrazine, THF, 10min (X120k).

E4. Pd-ppp (**8**·$(BArF)_8$), 130 eq Ru, 0.2 eq pyrazine, THF, 10min.

A

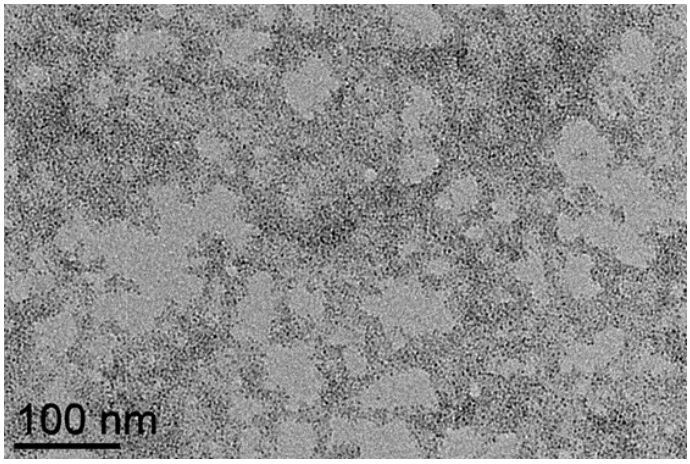

B

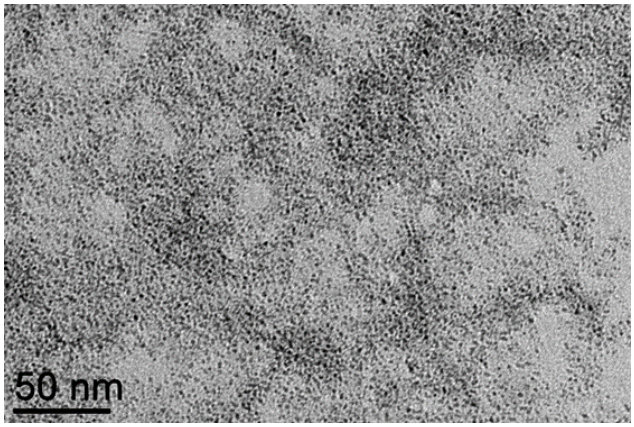

Figure S4. E4. Pd-ppp (**8**·$(BArF)_8$), 130 eq Ru, 0.2 eq pyrazine, THF, 10min. (A) X40k, (B) X80k.

E5. Pd-ppp (**8**·$(BArF)_8$), 40 eq Ru, 0.2 eq pyrazine, THF, 10min.

A

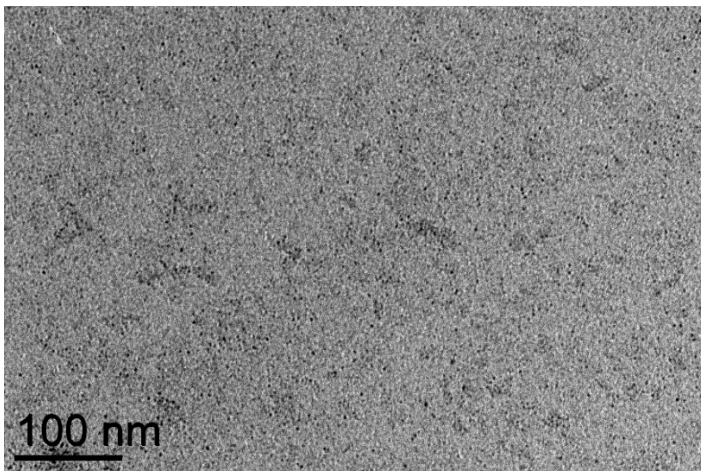

B

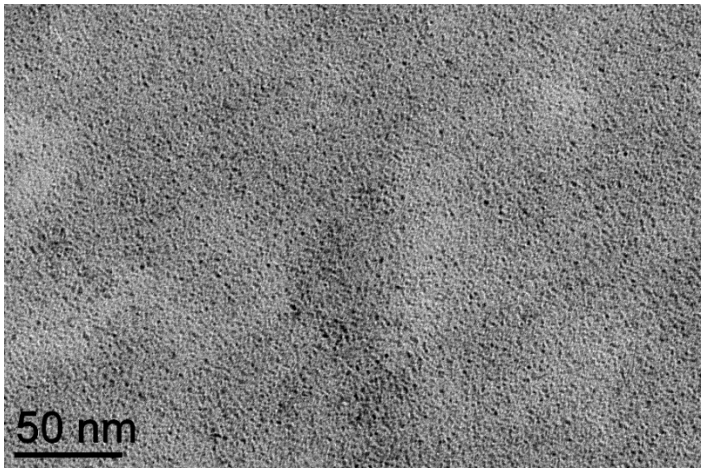

C

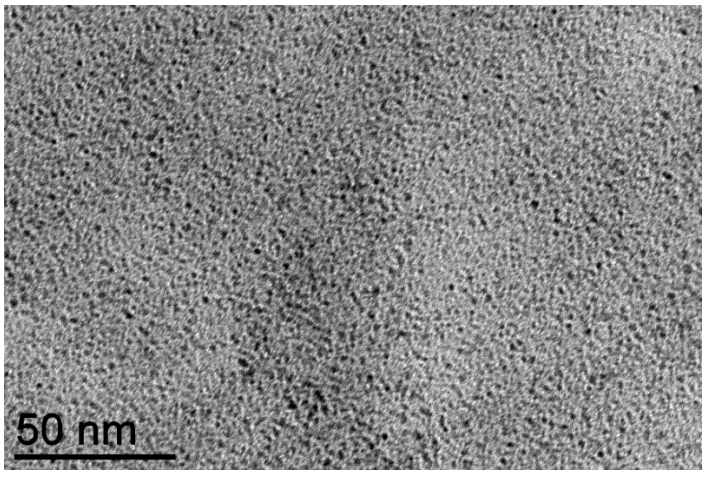

Figure S5. E5. Pd-ppp (**8**·$(BArF)_8$), 40 eq Ru, 0.2 eq pyrazine, THF, 10min. (A) X40k, (B) X80k, (C) 120k.

E6. Pd-ppp (**8**·$(BArF)_8$), 20 eq Ru, 0.2 eq pyrazine, THF, 10min.

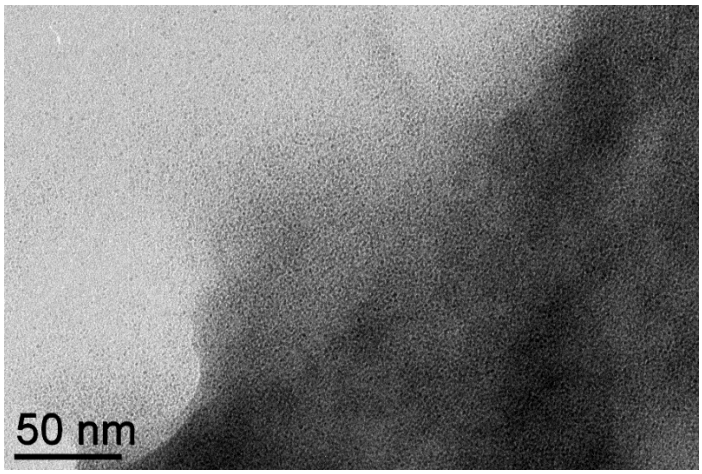

Figure S6. E6. Pd-ppp (**8**·$(BArF)_8$), 20 eq Ru, 0.2 eq pyrazine, THF, 10min (X80k).

E7. Pd-ppp (**8**·$(BArF)_8$), 200 eq Ru, 0.2 eq pyrazine, THF, 2min.

A

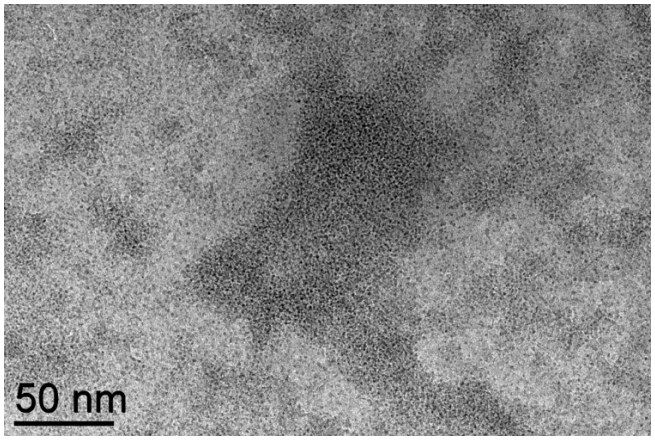

B

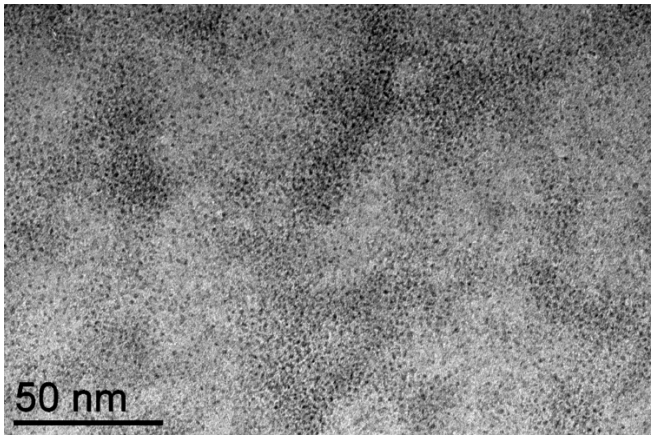

Figure S7. E7. Pd-ppp (**8**·$(BArF)_8$), 200 eq Ru, 0.2 eq pyrazine, THF, 2min. (A) X80k, (B) X120k.

E8. Pd-ppp (**8**·$(BArF)_8$), 130 eq Ru, 0.2 eq pyrazine, THF, 2min.

A

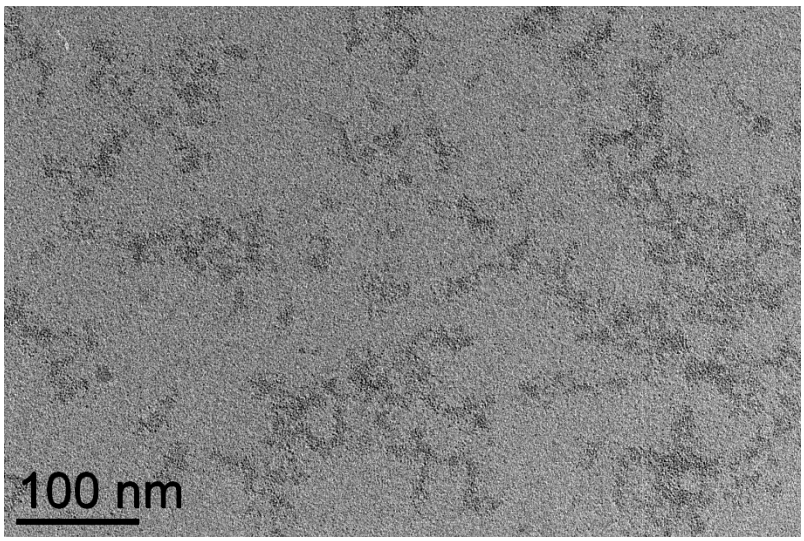

B

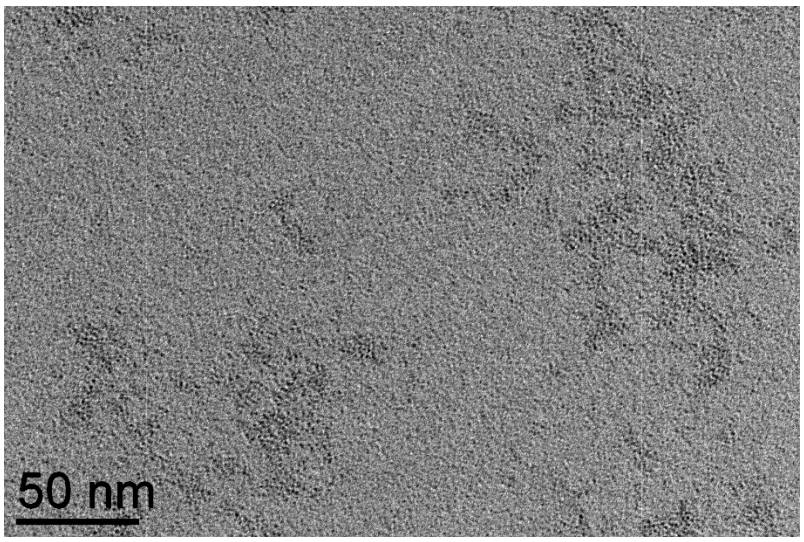

Figure S8. E8. Pd-ppp (**8**·$(BArF)_8$), 130 eq Ru, 0.2 eq pyrazine, THF, 2min. (A) X40k, (B) X80k.

E9. Pd-ppp (**8**·$(BArF)_8$), 80 eq Ru, 0.2 eq pyrazine, THF, 2min.

A

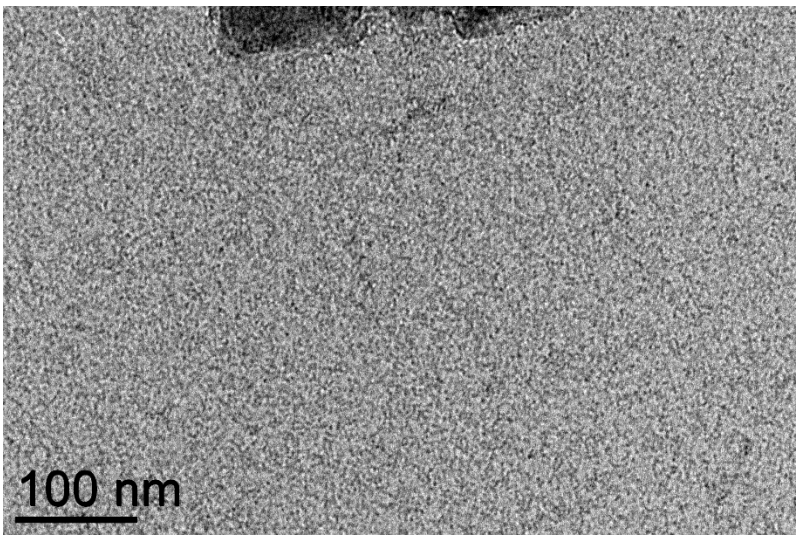

B

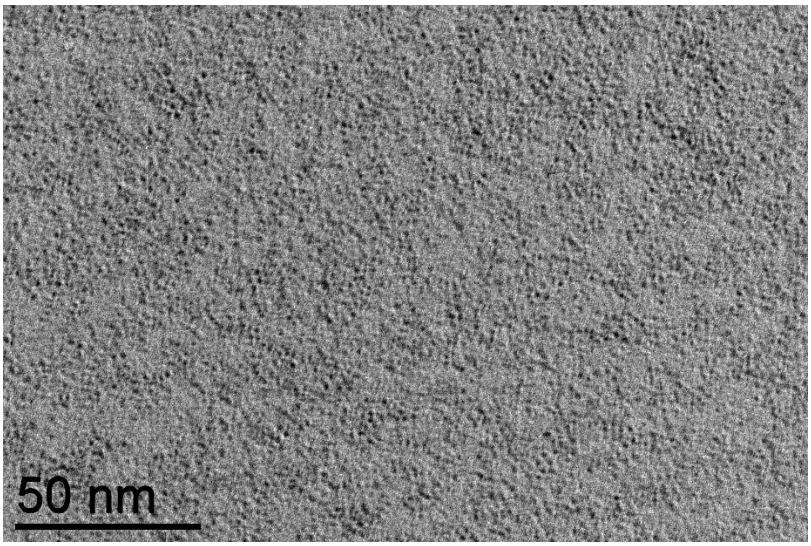

Figure S9. E9. Pd-ppp (**8**·$(BArF)_8$), 80 eq Ru, 0.2 eq pyrazine, THF, 2min. (A) X40k, (B) X120k.

E10. Pd-ppp (**8**·$(BArF)_8$), 60 eq Ru, 0.2 eq pyrazine, THF, 2min.

A

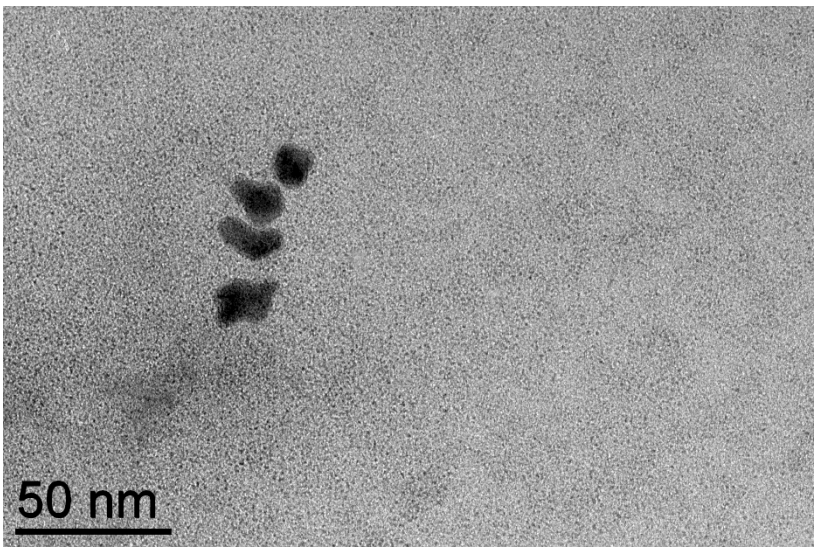

B

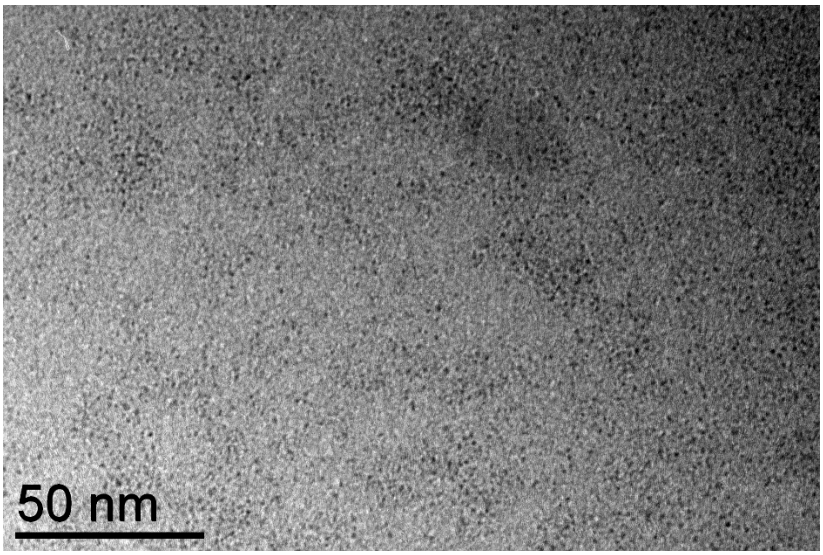

Figure S10. E10. Pd-ppp (**8**·$(BArF)_8$), 60 eq Ru, 0.2 eq pyrazine, THF, 2min. (A) X100k, (B) X120k.

E11. Pd-ppp (**8**·$(BArF)_8$), 40 eq Ru, 0.2 eq pyrazine, THF, 2min.

A

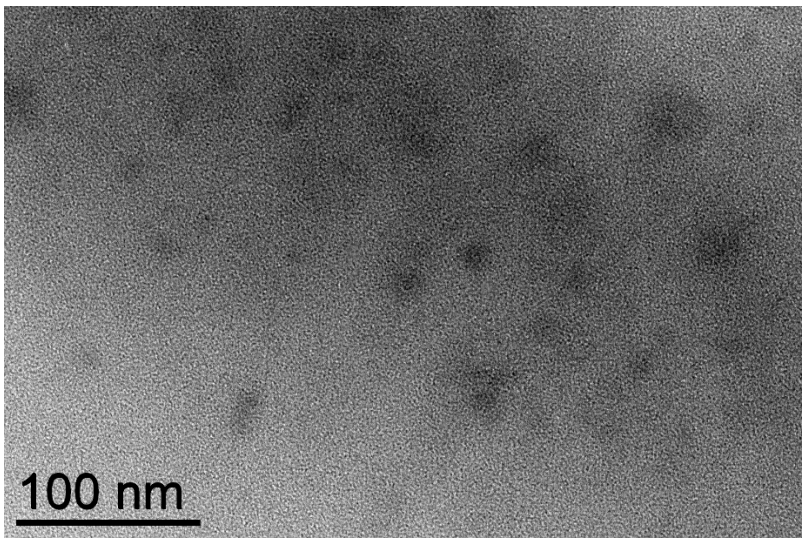

B

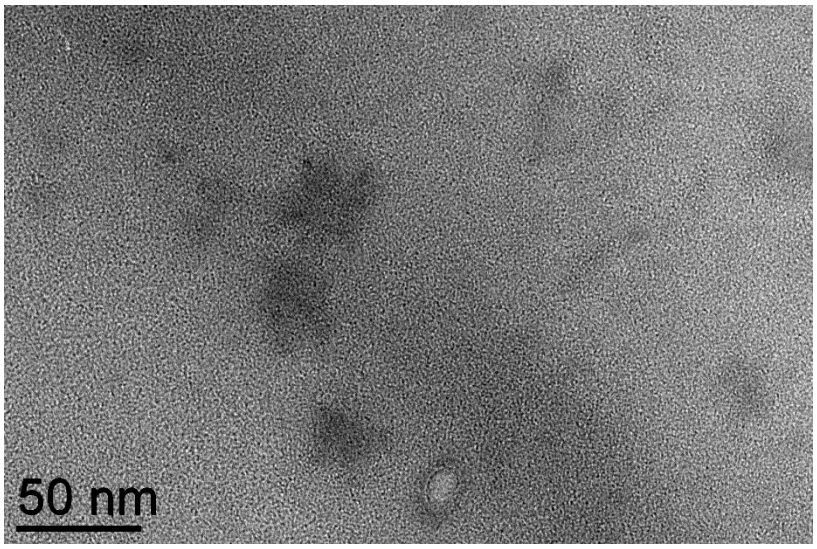

Figure S11. E11. Pd-ppp (**8**·$(BArF)_8$), 40 eq Ru, 0.2 eq pyrazine, THF, 2min. (A) X60k, (B) X80k.

E12. Pd-ppp (**8**·$(BArF)_8$), 130 eq Ru, 1 eq pyrazine, THF, 2min.

A

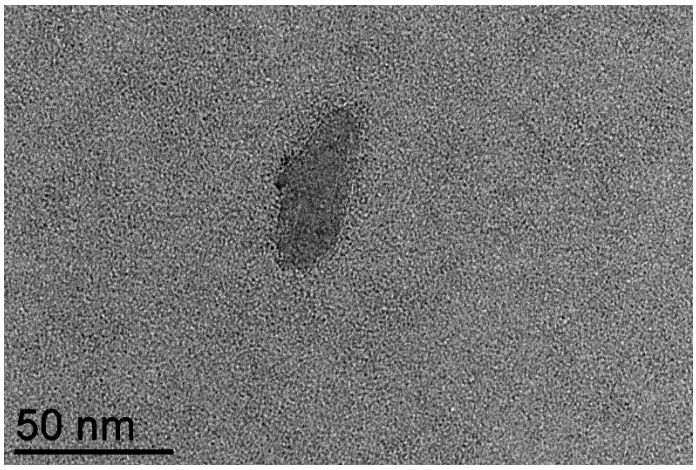

B

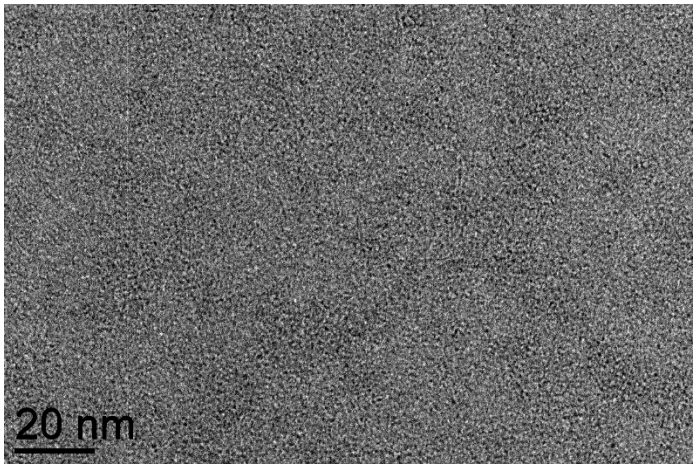

C

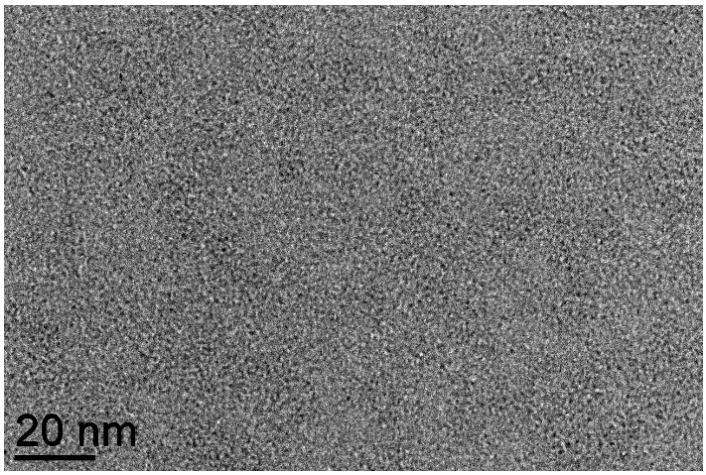

Figure S12. E12. Pd-ppp (**8**·$(BArF)_8$), 130 eq Ru, 1 eq pyrazine, THF, 2 min. (A) X120k, (B) X150k, (C) 150k.

E13. Pd clip ([$Pd_2(Me_2ppp)(AcO)_2$]$(OTf)_2$), 32 eq Ru, 0.2 eq pyrazine, THF (drops MeCN), 10min.

A

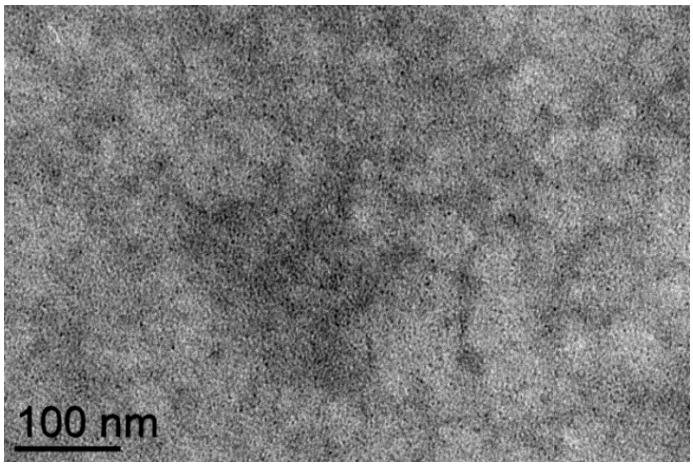

B

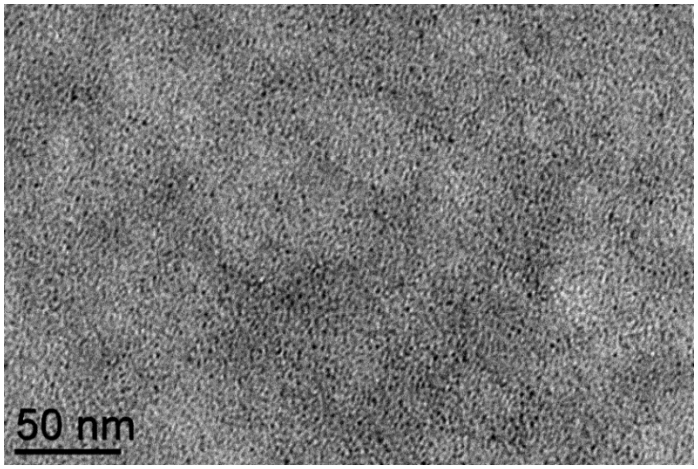

C

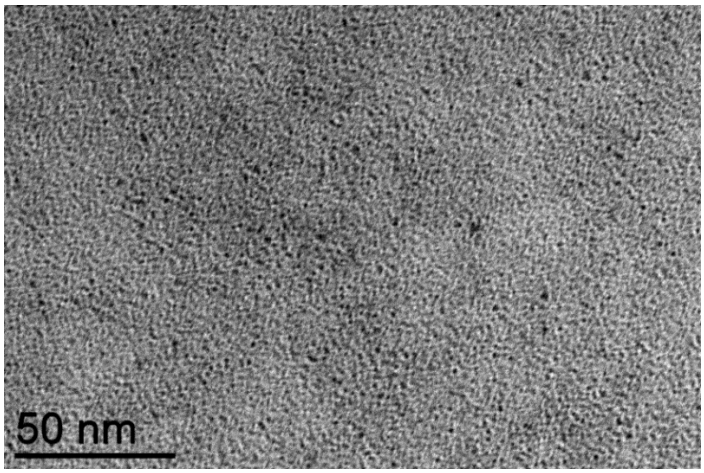

Figure S13. E13. Pd clip ([$Pd_2(Me_2ppp)(AcO)_2$]$(OTf)_2$), 32 eq Ru, 0.2 eq pyrazine, THF (drops MeCN), 10min. (A) X40k, (B) X80k, (C) X120k.

E14. Porf Zn (Zn-TCPP), 65 eq Ru, 0.2 eq pyrazine, THF (drops DMF), 10min.

A

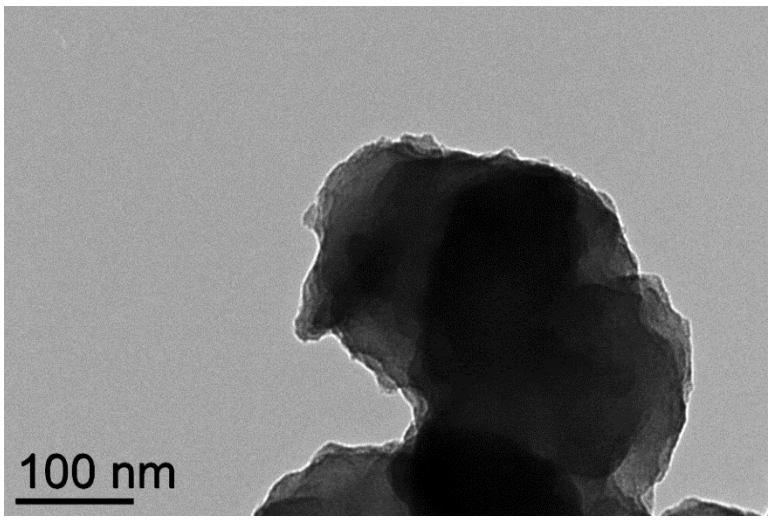

Figure S14. E14. Porf Zn (Zn-TCPP), 65 eq Ru, 0.2 eq pyrazine, THF (drops DMF), 10min. (A) X40k.

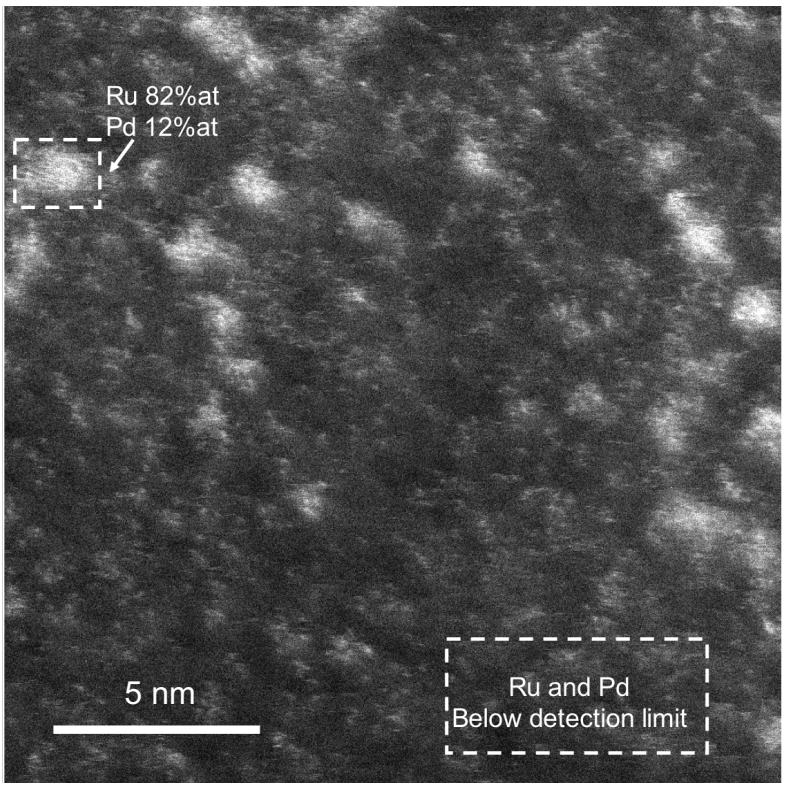

Figure S15. HR-TEM-EDX characterization corresponding to E2.

2.2. Ru NPs size distribution

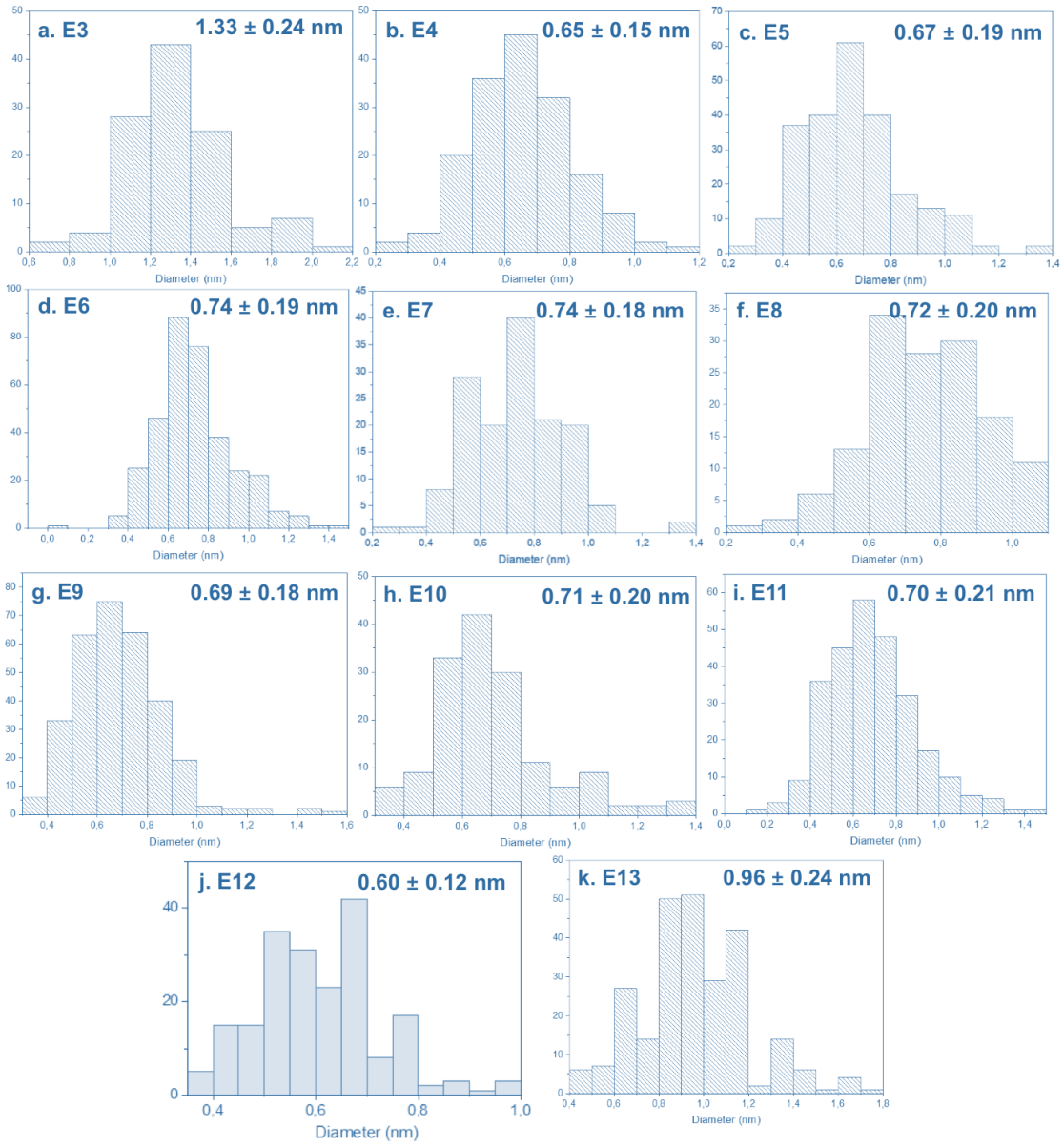

Figure S16. Ru NPs size distribution for E3 (**a**), E4 (**b**), E5 (**c**), E6 (**d**), E7 (**e**), E8 (**f**), E9 (**g**). E10 (**h**), E11 (**i**), E12 (**j**) and E13 (**k**).

2.3. Ru NPs characterization by HRMS

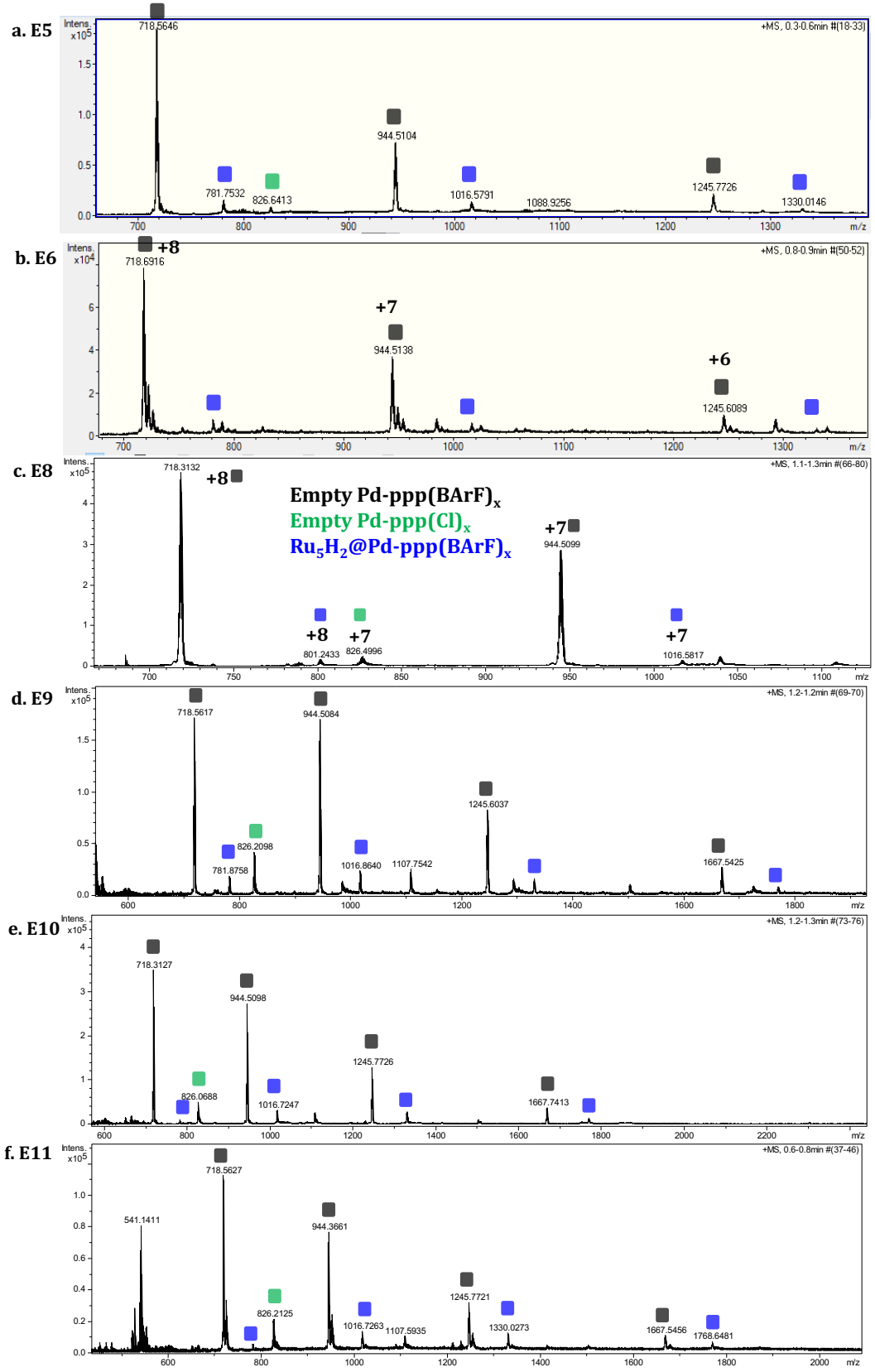

Figure S17. HR-ESI-MS of final experiment solutions. Recoveries of the nanocapsule were 95% for E6, 40% for E5, >98% for E8, 40% for E11, 76% for E9 and 82% for E10.

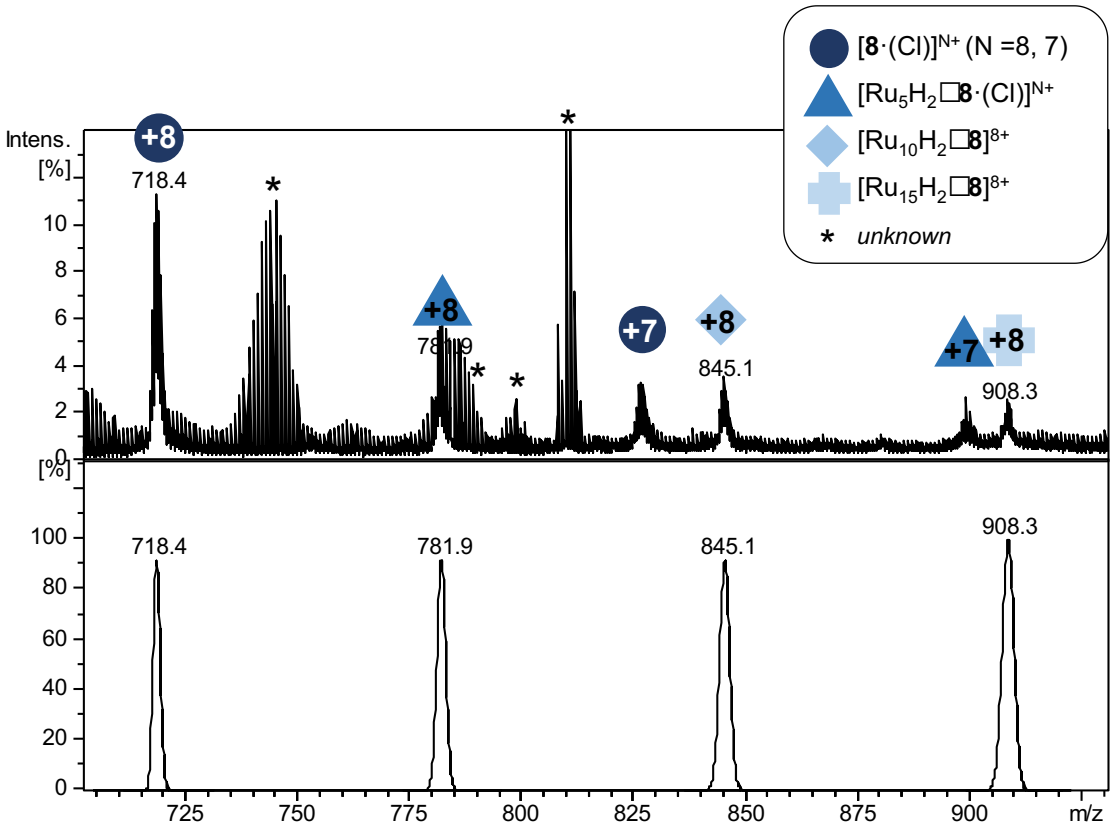

Figure S18. HR-ESI-MS of experiment E4 containing nanocapsule **8**·$(BArF)_8$ peaks filed with Ru_5H_2, $Ru_{10}H_2$ and $Ru_{15}H_2$.

2.4. X-ray diffraction of Cu-ppp clip

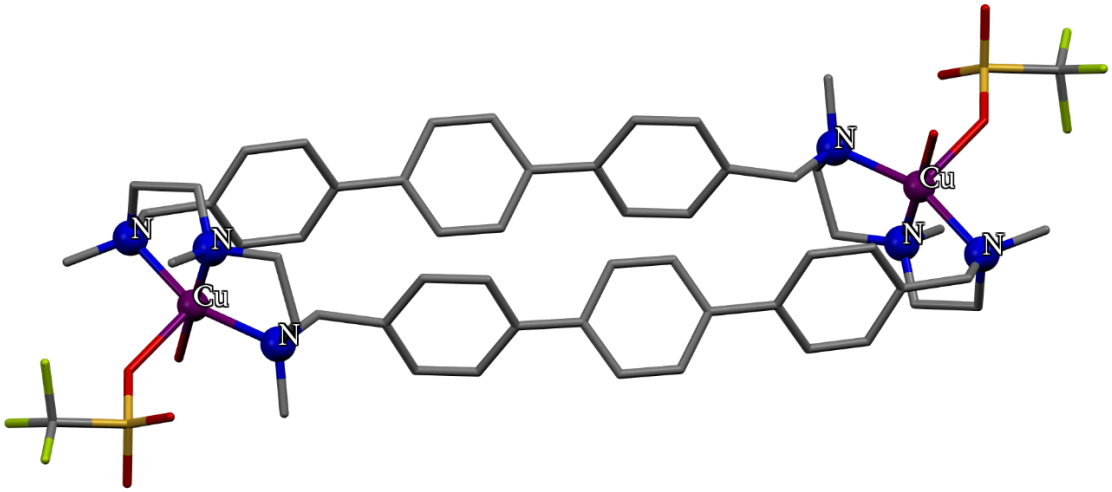

Figure S19. Crystal structure of macrocyclic compound $[Cu_2(Me_2ppp)(OTf)_2](OTf)_2$ (**CCDC 2127407**), synthesized following a reported procedure.[2] H atoms were omitted for clarity. Cu(II) presents a d^8 electronic configuration which enhance copper ions to adopt a tetracoordinated square-planar geometry formed by three N atoms of the macrocyclic ligand (Me_2ppp). Two H_2O molecules from the solvent were coordinated in a monodentate mode. Analogue structure is envisioned for the Pd clip ($[Pd_2(Me_2ppp)(AcO)_2](OTf)_2$)[2] used in this work (see experiment E12).

3. Supplementary Tables

Table S1. XRD data for $[Cu_2(Me_2ppp)(OTf)_2](OTf)_2$. (CCDC 2127407)

	$[Cu_2(Me_2ppp)(OTf)_2](OTf)_2$
CCDC code	EUL6P167_6_2on
formula	$C_{58}H_{76}Cu_2F_{12}N_6O_{17}S_4$
fw	1612.56
Crystal system	Monoclinic
Space group	C 1 2/c 1
a (Å)	31.531(5)
b (Å)	16.223(2)
c (Å)	17.453(2)
α (deg)	90
β (deg)	121.297(8)
γ (deg)	90
V (Å^3)	7629.(2)
Z	4
Dc (Mg m^{-3})	1.404
T (K)	100
λ (Å)	0.71076
μ (mm-1)	0.760
2ϑ *max (deg)*	25.01
reflns collected	46113
indep. reflns	6578
params	463
GOF on F^2	1.982
$R_{indices\ (I>2\sigma(I))}$	0.1455
$R_{indices\ (all\ data)}$	0.1923

4. DFT results and analysis of the Ru clusters and NP

4.1 Computational details

DFT calculations of metal nanoclusters. Software: Vienna ab initio simulation package, VASP;[5, 6] spin polarized DFT; exchange-correlation potential approximated by the generalized gradient approach proposed by Perdew, Burke, and Ernzerhof (PBE);[7, 8] projector augmented waves (PAW) full-potential reconstruction;[9, 10] PAW data sets for Ru treating the (*n*-1)*p*, (*n*-1)*d* and *n*s states (i.e. 14 valence electrons); kinetic energy cutoff: 500 eV; Γ-centered calculations;[11] Gaussian smearing (σ) of 0.02 eV width, energies being therefore extrapolated for σ = 0.00 eV; geometry optimization threshold: residual forces on any direction less than 0.02 eV/Å; supercell size: 26Å~26Å~29 $Å^3$ for all species and 28Å~32Å~22 $Å^3$ for $Ru_{57}H_{44}$ stabilized by the pillars model (ensures a vacuum space of at least ca. 10 Å between periodic images of the nanoclusters).

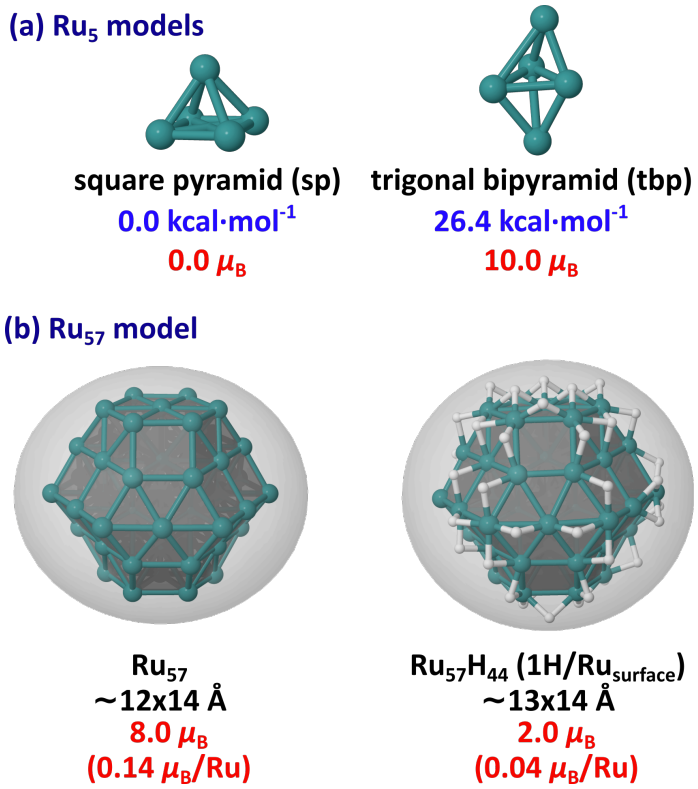

Figure S20. (a) Square pyramid (**sp**) and trigonal bipyramid (**tb**) Ru_5 models. Their relative energy (blue, in kcal/mol) and magnetic moment (red) are reported below. (b) bare Ru_{57} NP and its hydrogenated counterpart, with $1H/Ru_{surface}$. The approximate diameter of the spheroidal shape accounts for the van der Waals radius of atoms (H: ~120 pm; Ru: ~180 pm, see also Ref.[12]); the two numbers are the a and c diameters of the ellipsoid.

Ru_5 models: the **sp** and **tb** models are reported in Figure S18a.
Ru_{57} model : The model is an hcp spheroid with a diameter of ~1nm . Its structure is reported in Figure S18b.
Adsorption energies.

$$E_{\mathrm{ads}}(\mathrm{H}) = \frac{1}{n}\left[E(n\mathrm{H}^*) - E(\mathrm{NP}) - \frac{n}{2}E(\mathrm{H_2})\right] \quad (1)$$

$$E_{\mathrm{ads}}(\mathrm{L}) = \frac{1}{n}\left[E(n\mathrm{L}^*) - E(\mathrm{NP}) - nE(\mathrm{L})\right] \quad (2)$$

i.e. in the case of hydrides it is a dissociative adsorption energy.

Ab initio thermodynamics. The method and a review of applications to surface science was published in Ref.[13]. Let us consider the adsorption process of one species, L, which is the starting point of the Langmuir–Hinshelwood mechanism in heterogeneous catalysis. It can be summarized as: M + nL → nL* (M = metal cluster or nanoparticle and * stands for "chemisorbed") and the Gibbs free energy for this reaction is calculated as:

$$\Delta G_{\mathrm{ads}}(\mathrm{L}, T, p) = \left[\Delta G^{\circ} - n\mu(\mathrm{L})\right]/A \quad (3)$$

where A is the surface area of the metal cluster or NP, μ is the chemical potential of the L ligand and ΔG° is calculated after DFT energies and vibrational contributions to energies. The free energy diagram reported in Figure 10 of the manuscript was calculated with our in-house *aithermo* software.[14] Methodological details and examples of applications done by some of us can be found in Refs.[14-18].

Second order energy differences. The second–order energy difference Δ_2E is well known to be an important stability criterion in cluster science.[19, 20] In the present case, it is defined as:

$$\Delta_2 E(n) = E(n+1) + E(n-1) - 2E(n) \quad (4)$$

where E(*n*) is the energy of the most stable $Ru_5H_n(\eta^6\text{-PhH})_2(\eta^6\text{-pyz})_3$ isomer.
It reflects the stability of a Ru_5H_n cluster with respect to Ru_5H_{n+1} and Ru_5H_{n-1} species, the higher Δ_2E(*n*)
the more stable the cluster of size n. It usually exhibits an odd-even alternation.

4.2 Additional DFT results

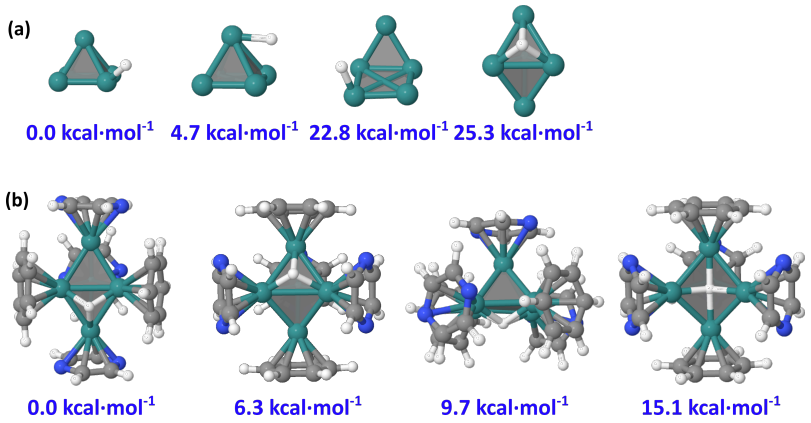

Figure S21. (a) Bare Ru_5H isomers; (b) $Ru_5H(\eta^6\text{-PhH})_2(\eta^6\text{-pyz})_3$ isomers. Relative energies in blue.

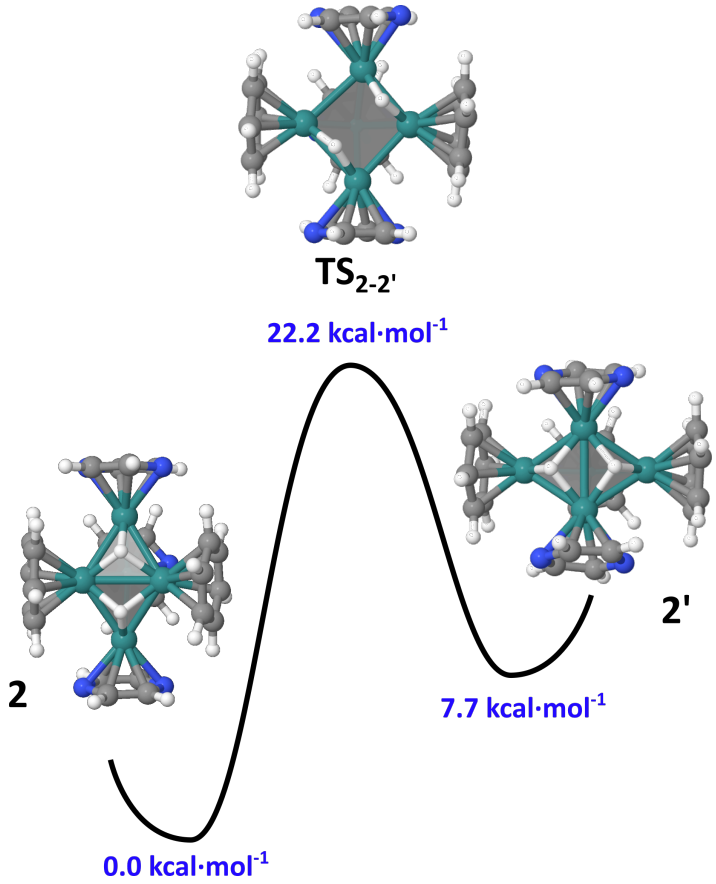

Figure S22. Isomerization pathway of the **bp**-$Ru_5H_2(\eta^6\text{-PhH})_2(\eta^6\text{-pyz})_3$ cluster, via an **sp**-$Ru_5H_2(\eta^6\text{-PhH})_2(\eta^6\text{-pyz})_3$ transition state. **2**: two equatorial pyz, one equatorial PhH and two axial pyz; **2'**: 3 equatorial pyz and two axial PhH.

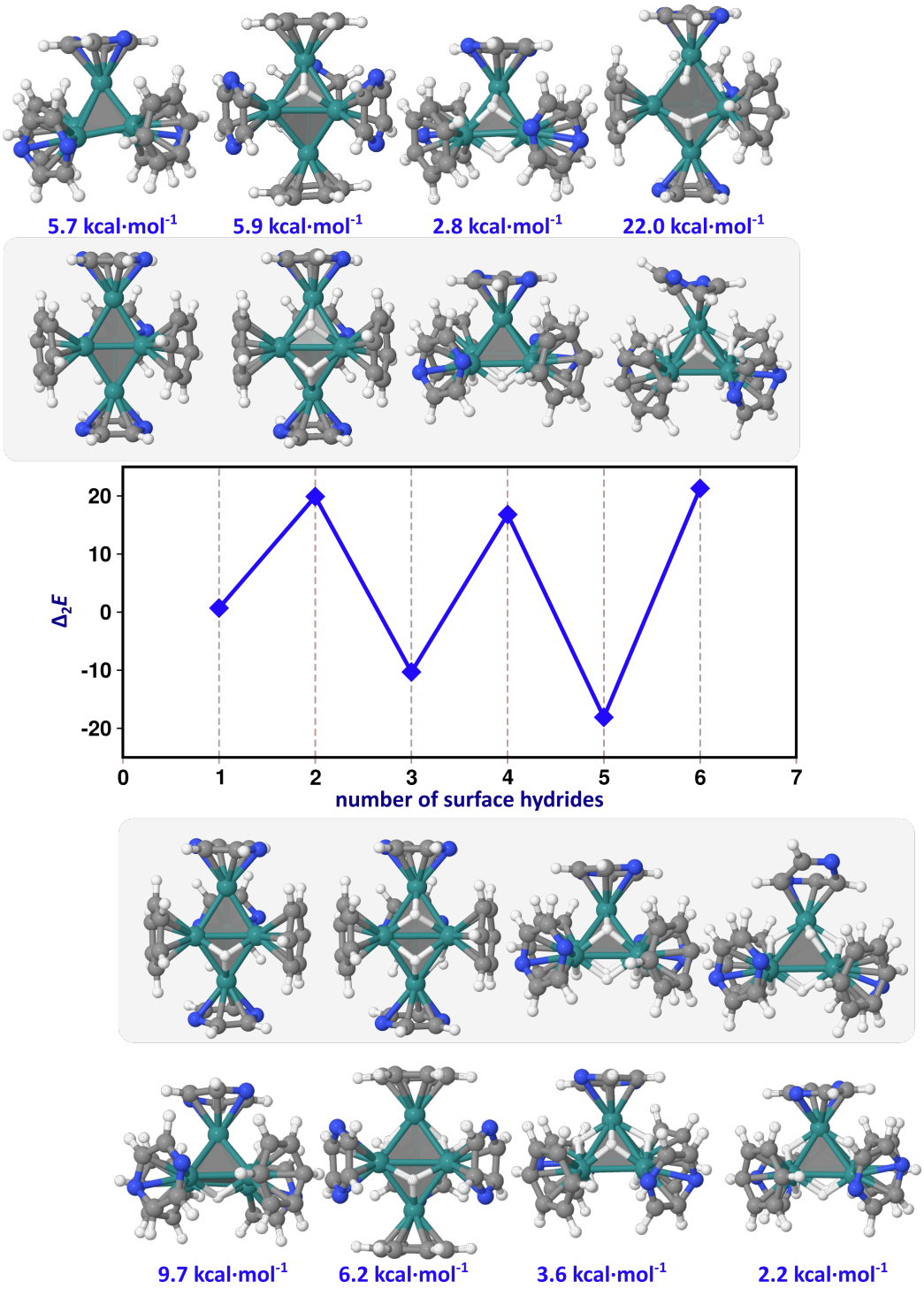

Figure S23. Second-order energy differences for the most stable $Ru_5H_n(PhH)_2(pyz)_3$ isomer, *n*=1-6 (structures on a grey background). Even-*n* closed-shell clusters are more stable than the radical odd-*n* clusters, as expected. The second low-lying isomer found in this study is also shown for each size, with its energy (in blue) relative to the lowest one.

5. Supplementary References

1. E. Ubasart, O. Borodin, C. Fuertes-Espinosa, Y. Xu, C. García-Simón, L. Gómez, J. Juanhuix, F. Gándara, I. Imaz, D. Maspoch, M. von Delius and X. Ribas, *Nat. Chem.*, 2021, **13**, 420-427.
2. E. Ubasart, C. García-Simón, M. Pujals, K. Asad, N. Chronakis, T. Parella and X. Ribas, *Org. Chem. Front.*, 2021, **8**, 4101-4105.
3. L. M. Martínez-Prieto and B. Chaudret, *Acc. Chem. Res.*, 2018, **51**, 376-384.
4. L. M. Martínez-Prieto, C. Urbaneja, P. Palma, J. Cámpora, K. Philippot and B. Chaudret, *Chem. Commun.*, 2015, **51**, 4647-4650.
5. G. Kresse and J. Furthmüller, *Phys. Rev. B*, 1996, **54**, 11169-11186.
6. G. Kresse and J. Furthmüller, *Comput. Mater. Sci.*, 1996, **6**, 15-50.
7. J. P. Perdew, K. Burke and M. Ernzerhof, *Phys. Rev. Lett.*, 1996, **77**, 3865-3868.
8. J. P. Perdew, K. Burke and M. Ernzerhof, *Phys. Rev. Lett.*, 1997, **78**, 1396-1396.
9. P. E. Blöchl, *Phys. Rev. B*, 1994, **50**, 17953-17979.
10. G. Kresse and D. Joubert, *Phys. Rev. B*, 1999, **59**, 1758-1775.
11. H. J. Monkhorst and J. D. Pack, *Phys. Rev. B*, 1976, **13**, 5188-5192.
12. S. S. Batsanov, *Inorg. Mater.*, 2001, **37**, 871-885.
13. K. Reuter, C. Stampf and M. Scheffler, in *Handbook of Materials Modeling: Methods*, ed. S. Yip, Springer Netherlands, Dordrecht, 2005, DOI: 10.1007/978-1-4020-3286-8_10, pp. 149-194.
14. L. Cusinato, I. del Rosal and R. Poteau, *Dalton Trans.*, 2017, **46**, 378-395.
15. I. del Rosal, L. Truflandier, R. Poteau and I. C. Gerber, *J. Phys. Chem. C*, 2011, **115**, 2169-2178.
16. L. Cusinato, L. M. Martínez-Prieto, B. Chaudret, I. del Rosal and R. Poteau, *Nanoscale*, 2016, **8**, 10974-10992.
17. R. González-Gómez, L. Cusinato, C. Bijani, Y. Coppel, P. Lecante, C. Amiens, I. del Rosal, K. Philippot and R. Poteau, *Nanoscale*, 2019, **11**, 9392-9409.
18. N. Rothermel, H.-H. Limbach, I. del Rosal, R. Poteau, G. Mencia, B. Chaudret, G. Buntkowsky and T. Gutmann, *Catal. Sci. Tech.*, 2021, **11**, 4509-4520.
19. W. D. Knight, K. Clemenger, W. A. de Heer, W. A. Saunders, M. Y. Chou and M. L. Cohen, *Phys. Rev. Lett.*, 1984, **52**, 2141-2143.
20. R. Poteau and F. Spiegelmann, *J. Chem. Phys.*, 1993, **98**, 6540-6557.